Electronic Supplementary Material (ESI) for Nanoscale.
This journal is © The Royal Society of Chemistry 2020

Supporting Information

Towards enhanced sodium storage of anatase TiO_2 via a dual-modification approach of Mo doping combined with AlF_3 coating

Xue Bai,[bc] Tao Li,*[cd] Umair Gulzar,[cd] Eleonora Venezia,[c] Lin Chen,[c] Simone Monaco,[c] Zhiya Dang,[c] Mirko Prato,[c] Sergio Marras,[c] Pejman Salimi Naden,[c] Silvio Fugattini,[c] Claudio Capiglia[e] and Remo Proietti Zaccaria*[ac]

[a] Cixi Institute of Biomedical Engineering, Ningbo Institute of Materials Technology and Engineering, Chinese Academy of Sciences, Ningbo 315201, China

[b] College of Materials Science and Engineering, Shandong University of Science and Technology, Qingdao 266590, China

[c] Istituto Italiano di Tecnologia, via Morego 30, Genova 16163, Italy

[d] DIBRIS, University of Genova, via Opera Pia 13, Genova 16145, Italy

[e] Nagoya Institute of Technology, Gokiso-cho, Showa-ku, Nagoya, Aichi, 466-8555, Japan

*Corresponding author. E-mail: Tao.Li@iit.it, Remo.Proietti@iit.it, Remo.Proietti@nimte.ac.cn

Table S1 Calculated lattice parameters *a*, *c* and crystalline size of the as-prepared TO and MTO samples. The whole powder pattern decomposition (WPPD) analysis, based on Pawley method, was carried out to determine the cell parameters, average size of the crystalline domains and strain of both the undoped and doped samples. Instrumental broadening was calculated using a NIST SRM 660c LaB6 powder.

	a=*b* (Å)	*c* (Å)	Crystalline size (nm)	Strain (%)
TO (pure TiO_2)	3.7867	9.5051	20.0	0.294
MTO (5% doped)	3.7878	9.4946	16.2	0.342

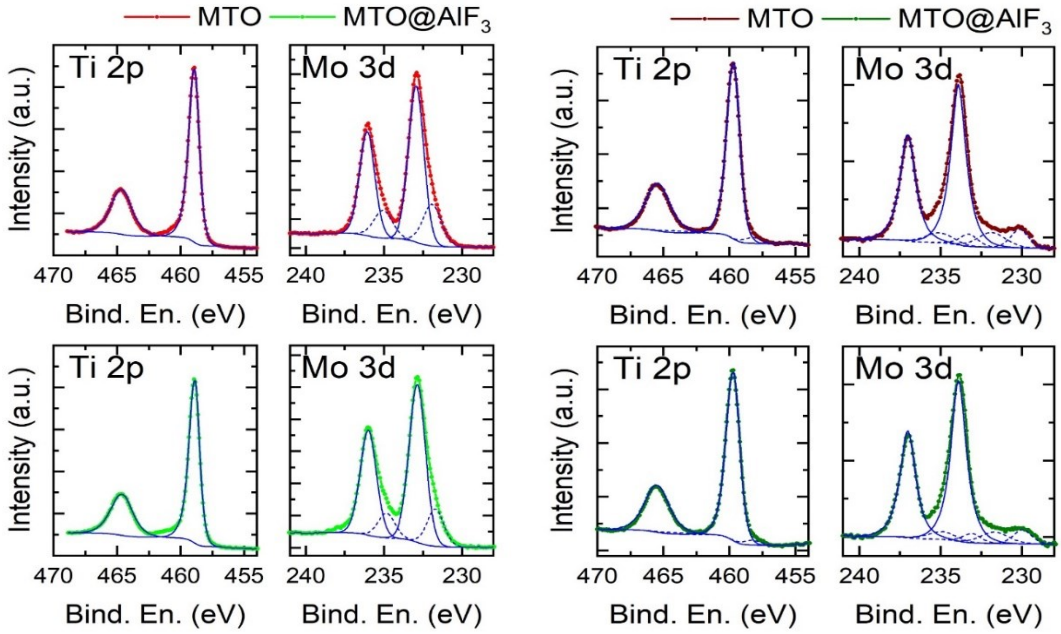

Fig. S1 XPS of MTO and MTO@AlF_3 before cycling (left) and after cycling (right).

Fig. S1 left shows the comparison of Ti 2p and Mo 3d spectra collected on the MTO and the MTO@AlF_3 samples before cycling. XPS data suggest that the procedure used for realizing the AlF3

coating on the surface of the MTO particles did not affect the oxidation states of neither Ti nor Mo. Indeed, in both samples, the Ti 2p spectrum is characterized by the Ti $2p_{3/2}$ and Ti $2p_{1/2}$ peaks located at (458.7±0.2) eV and (464.4±0.2) eV, typical of Ti(IV) oxide [1]. For both cases, Mo 3d spectra could be fitted by a couple of doublets; the most intense doublet, with Mo $3d_{5/2}$ and Mo $3d_{3/2}$ peaks at (232.6±0.2) eV and (235.7±0.2) eV, is indicative of Mo(VI) species [2], while the less intense one, with Mo $3d_{5/2}$ and Mo $3d_{3/2}$ peaks at (231.6±0.2) eV and (234.7±0.2) eV, could be attributed to Mo(V) species [3]. The main difference between the two samples is the [Mo(V)]/[Mo(VI)] ratio, equal to 0.3 and to0.2 for the MTO and MTO@AlF_3 samples, respectively. Finally, it is observed that the presence of surface fluorides could have induced a higher oxidation of Mo in MTO@AlF_3.

When it comes to MTO@AlF_3 after cycling, the results are summarized in Fig. S1 right. The figure shows the comparison of Ti 2p and Mo 3d spectra collected on the MTO and the MTO@AlF_3 samples, after cycling. Also in this case, XPS data indicate that the oxidation states of Ti and Mo in the two samples are similar, even after their use in Na-ion batteries, as the Ti 2p and Mo 3d spectra are almost the same.

In both samples, the Ti 2p spectrum is characterized by the Ti $2p_{3/2}$ and Ti $2p_{1/2}$ peaks located at (459.8±0.2) eV and (465.5±0.2) eV. The positions are approx. 1 eV higher than those measured on the starting materials, most likely because of the presence of a high concentration of fluorine in the sample (due to the PVDF binder used in the preparation of the electrodes). With this in mind, we assigned the observed peaks to Ti(IV) oxide. For both samples, the best fit of the Ti 2p spectra was obtained by adding also a second doublet of peaks, with Ti $2p_{3/2}$ and Ti $2p_{1/2}$ peaks located at (458.3±0.2) eV and (464.0±0.2) eV, i.e., at approx. 1.5 eV below the Ti(IV) peaks. We therefore assigned this minor intensity doublet to Ti(III) species [1].

Mo 3d spectrum in both cases is dominated by a doublet with Mo $3d_{5/2}$ and Mo $3d_{3/2}$ peaks at (233.9±0.2) eV and (237.0±0.2) eV, that we assigned to Mo(VI) species, even if shifted to higher energies with respect to what measured on the starting materials. Again, we assign the shift to the electron-withdrawal effect due to the presence of high amounts of highly electronegative fluorine species from PVDF. To obtain the best fit, we had to add in both cases also other four peaks, which could be assigned to Mo(IV) species, according to [4].

With respect to the before cycling materials, it is interesting to notice that both Ti and Mo show the presence of reduced species (i.e., Ti(III) and Mo(IV)), likely due to a partial residue of Na^+ in the

material after “sodiation”, inducing therefore Ti and Mo reduction in order to maintain charge neutrality in the system.

Finally, when looking at the effect of AlF_3 on SEI formation, XPS data (not shown here) depict a higher presence of C-related components in case of absence of AlF_3. This result suggests that AlF_3 might mitigate the SEI formation with an overall positive influence on the cell. However, a detailed and dedicated study in this direction would be necessary before reaching any clear conclusion as the binder contribution to the C-related peaks could change from sample to sample. In this respect, it should be setup a standardization for the washing procedure in order to guarantee a proper reading and interpretation of the C-peaks in the XPS analysis.

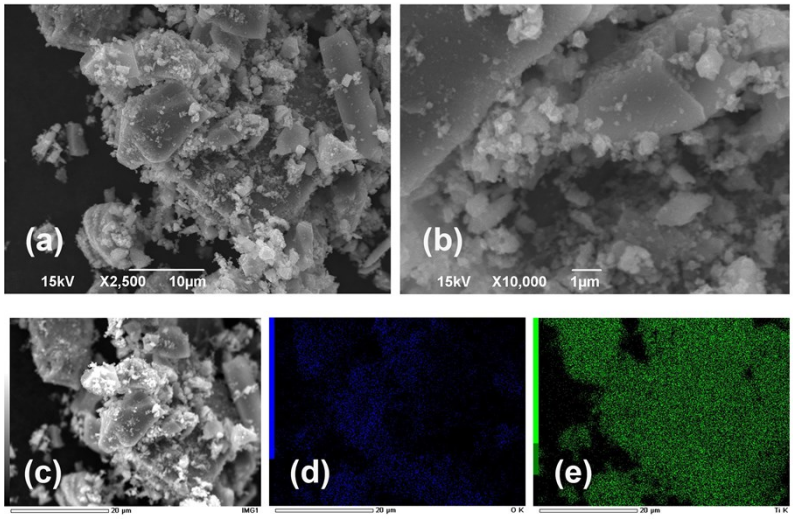

Fig. S2 (a, b) SEM images of TO and the corresponding EDS elemental mappings of (d) O and (e) Ti, referred to image (c).

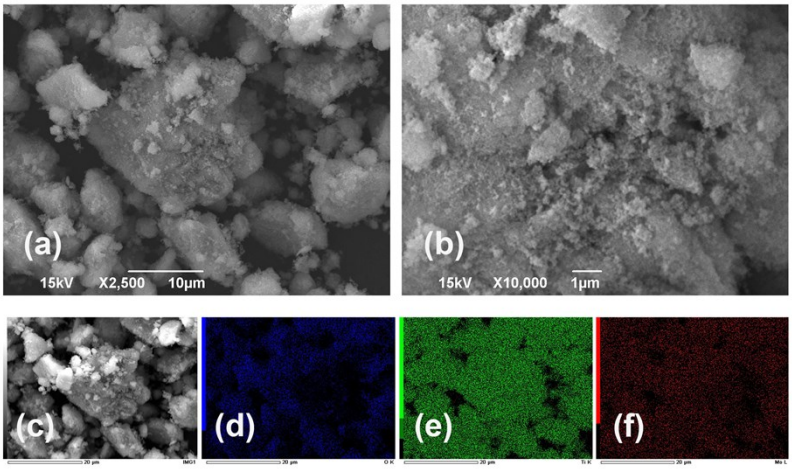

Fig. S3 (a, b) SEM images of MTO and the corresponding EDS elemental mappings of (d) O and (e) Ti and (f) Mo, referred to image (c).

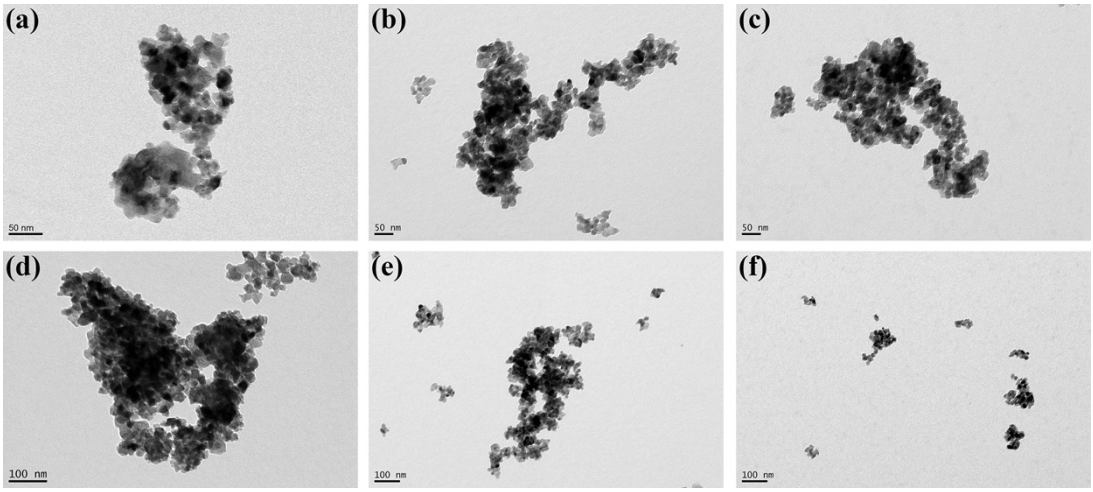

Fig. S4 TEM images of (a, d) TO, (b, e) MTO, and (c, f) MTO@AlF_3.

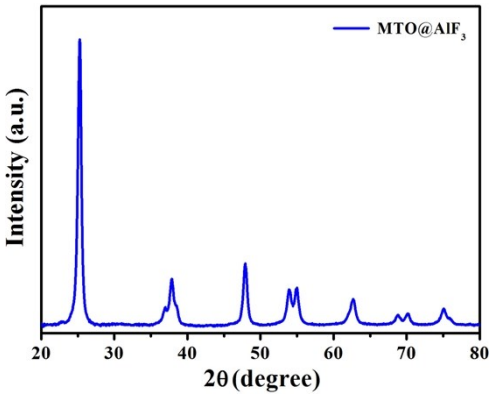

Fig. S5 XRD pattern of the MTO@AlF_3 sample (with AlF_3 content of 1wt%).

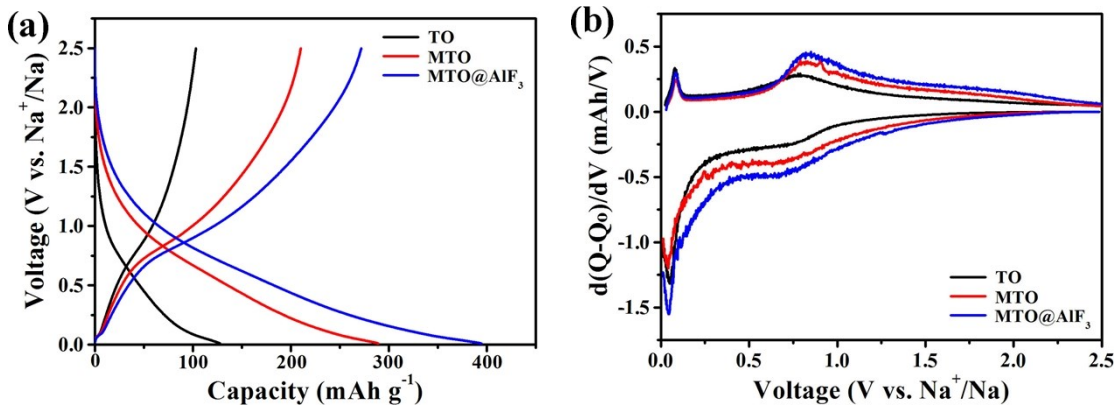

Fig. S6 (a) Galvanostatic discharge−charge voltage curves for the 2nd cycle at 0.1 C between 0.01 and 2.5 V, (b) the corresponding differential capacity (d*Q*/d*V*) *vs.* voltage plots of TO, MTO, and MTO@AlF_3.

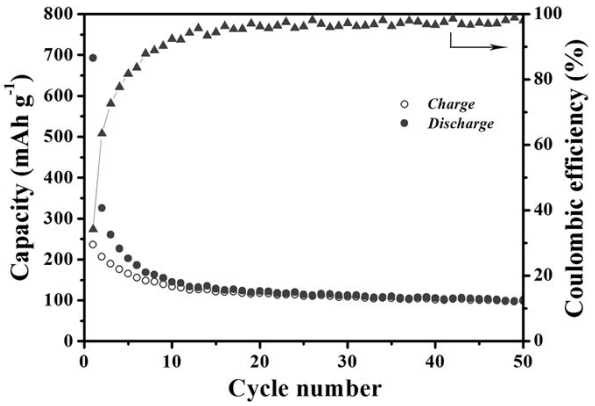

Fig. S7 Cycling performance of 3wt%-AlF_3 coated MTO sample at 0.1C.

Table S2 Brief summary of electrochemical performance for modified TiO_2 anodes via various preparation methods.

Materials	Preparation methods	Capacity/Current density (mAh g^{-1}/mA g^{-1})	Capacity at high rate (mAh g^{-1}/mA g^{-1})	Ref.
Nb-doped TiO_2 nanoparticles	sol-gel	177/33 (100 cycles)	108.8/1650	[S1]
Sn-doped TiO_2	sol-gel and	257/50	106/5000	[S2]

nanotubes	subsequent hydrothermal	(50 cycles)		
Fe-doped TiO_2/ amorphous carbon composite	wet chemistry process	304/100 (50 cycles)	198/2000	[S3]
Mo-doped TiO_2 nanoparticles	sol-gel	231.8/33.5 (100 cycles)	108.3/1680	[S4]
Co-doped TiO_2 nanodisks	solvothermal	170/100 (100 cycles)	121/1000	[S5]
N-doped TiO_2 nanorods	hydrothermal and ionic exchange	166/840 (300 cycles)	131/3360	[S6]
B-doped TiO_2 nanoparticles	sol-gel	225/33 (5 cycles)	147/660	[S7]
Carbon coated anatase TiO_2 mesocrystals	hydrothermal	201.3/168 (500 cycles)	90/3360	[S8]
N and S co-doped hollow CNF/S-doped anatase TiO_2	hydrothermal	193.8/100 (50 cycles)	120.9/1000	[S9]
Mo-doped TiO_2@AlF_3	co-precipitation	178.9/33.5 (50 cycles)	98.4/1675	This work

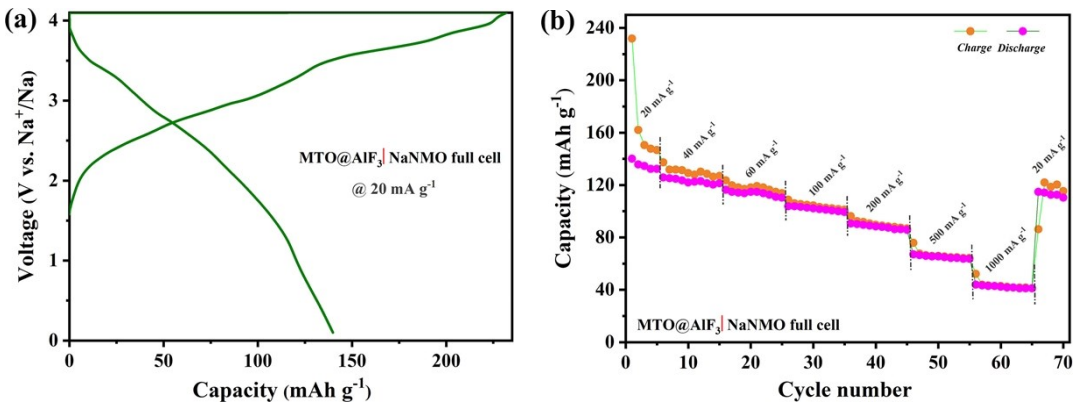

Fig. S8 (a) Galvanostatic charge−discharge voltage curves for the initial cycle of

MTO@AlF_3|NaNMO full cell between 0.1 and 4.1 V at specific current of 20 mA g^{-1}, (b) the rate performance of MTO@AlF_3|NaNMO full cell at different specific current of 20, 40, 60, 100, 200, 500, 1000 mA g^{-1} and eventually come back to 20 mA g^{-1}. The specific capacity is based on the reference of MTO@AlF_3.

Na-ion full cell assembling:

In order to validate MTO@AlF_3 anode material in Na-ion full cell, lab-made P2-type $Na_{2/3}Ni_{1/4}Mn_{3/4}O_2$ (NaNMO) was used as the cathode material to match with MTO@AlF_3 anode. The positive electrode was prepared by casting the mixed slurry of NaNMO nanoparticles (85 wt.%), super P carbon (10 wt.%), and polyvinylidene fluoride (5 wt.%) in N-methylpyrrolidone onto etched aluminum foil. The coating was calendered and further dried at 120 °C under vacuum for at least 2 hours before use. The balance calculation of the full cell was calculated based on the capacity ratio of Q_{Anode}:$Q_{Cathode}$ as 1.10. Accordingly, we designed the Na full cell by adjusting the mass loading of active material at negative and positive electrodes to 1:1.5. CR2032-type coin cells with NaNMO and MTO@AlF_3 as cathode and anode respectively, were assembled and sealed in the glovebox (H_2O and O_2 < 0.1ppm). 1.0 M of $NaClO_4$ in a mixture solvent of ethylene carbonate and propylene carbonate (1:1 by volume) was used as electrolyte, and glass filter (Whatman) was used as separator. It is noted that before the full cell assembly, negative electrode (electrode preparation process is given in Section 2.3 in the main text) was firstly cycled at 0.1C (33.5 mA g^{-1}) for two cycles to ensure a high reversibility of MTO@AlF_3 in a Na half-cell with a sodium metal disc used as counter and reference electrode. Then the cycled half-cell was disassembled in the glovebox and the working electrode was taken out for the subsequent full cell assembly. MTO@AlF_3|NaNMO full cell was charged/discharged using a constant current protocol in the voltage range of 0.1–4.1 V at different specific current of 20, 40, 60, 100, 200, 500, 1000 mA g^{-1} and eventually come back to 20 mA g^{-1}. All the measurements were done at room temperature. The electrochemical performance of the full cell is shown in **Fig. S8**. Interestingly, even though the initial cycle shows a strong irreversibility (Fig. S8a), it appears that the cell undergoes a kind of recovery upon cycling as emerging from Fig. S8b. The full cell delivers a discharge capacity of 139.9 mAh g^{-1} based on the reference of MTO@AlF_3 at a current density of 20 mA g^{-1} (Fig. S8a) and good rate capabilities (Fig. S8b), demonstrating its promising potential for energy storage systems.

References

[S1] F. Zhao, B. Wang, Y. Tang, H. Ge, Z. Huang and H. K. Liu, *J. Mater. Chem. A*, 2015, **3**, 22969-22974.

[S2] D. Yan, C. Yu, Y. Bai, W. Zhang, T. Chen, B. Hu, Z. Sun and L. Pan, *Chem. Commun.*, 2015, **51**, 8261-8264.

[S3] Y. Lai, W. Liu, J. Li, K. Zhang, F. Qin, M. Wang and J. Fang, *J. Alloys Compd.*, 2016, **666**, 254-261.

[S4] H. Liao, L. Xie, Y. Zhang, X. Qiu, S. Li, Z. Huang, H. Hou and X. Ji, *Electrochim. Acta*, 2016, **219**, 227-234.

[S5] Z. Hong, M. Kang, X. Chen, K. Zhou, Z. Huang and M. Wei, *ACS Appl. Mater. Interfaces*, 2017, **9**, 32071-32079.

[S6] Y. Yang, X. Ji, M. Jing, H. Hou, Y. Zhu, L. Fang, X. Yang, Q. Chen and C. E. Banks, *J. Mater. Chem. A*, 2015, **3**, 5648-5655.

[S7] B. Wang, F. Zhao, G. Du, S. Porter, Y. Liu, P. Zhang, Z. Cheng, H. Liu and Z. Huang, *ACS Appl. Mater. Interfaces*, 2016, **8**, 16009-16015.

[S8] W. Zhang, T. Lan, T. Ding, N. Wu and M. Wei, *J. Power Sources*, 2017, **359**, 64-70.

[S9] F. Li, W. Liu, Y. Lai, F. Qin, L. Zou, K. Zhang and J. Li, *J. Alloys Compd.*, 2017, **695**, 1743-1752.